Dipolar broadening of $I = \frac{1}{2}$ NMR spectra of solids

Jens Jensen
Ørsted Laboratory, Niels Bohr Institute, Universitetsparken 5, 2100 Copenhagen, Denmark
(Received 16 December 1994; revised manuscript received 30 May 1995)

The equations of motion of dipolar-coupled spins of $I = 1/2$ placed on a rigid lattice are solved approximately in the high-temperature and high-field limit. The NMR spectra predicted by this theory are in close agreement with both the theoretical spectral moments, up to the eighth in the case of a simple cubic lattice, and the extremely accurate experimental results which have been obtained in the case of CaF_2. The theory is compared with the recent NMR experiment of Lefmann *et al.* on ^{13}C diamond. It predicts a double-peak splitting of the NMR spectrum when the field is applied along [111], in accordance with the experiment, though the widths of the calculated resonance lines are smaller than observed.

I. INTRODUCTION

Recently Lefmann *et al.*[1] have measured the NMR spectra on single crystals of the new material ^{13}C diamond. The nuclear spin of the ^{13}C isotope is 1/2, and in the case of a field applied along [111], the square of the magnetic dipole-dipole interaction between two nearest-neighboring spins in the direction of the field is an order of magnitude stronger than the interaction between any other neighbors. This leads to a splitting of the resonance into two peaks, a phenomenon which has only previously been observed in dense systems of molecules.[2–4] The ^{13}C diamond constitutes a system of $I = 1/2$ nuclei interacting through the dipole force between their magnetic moments and, because the Debye temperature of the diamond crystal is high, the lattice may be considered to be rigid. The same model applies for the NMR in CaF_2 except that the $I = 1/2$ nuclei, the F ions, are placed on a simple cubic lattice.

The simplest problem of NMR in solids is the one where identical nuclei of $I = 1/2$ are placed on a rigid lattice. In this case no quadrupole moment or quadrupolar broadening effects have to be considered, and lattice vibrations are neglected. The calculation of the dipolar broadening of the NMR is, nevertheless, a complicated many-body problem with no small expansion parameter. Van Vleck calculated the second and fourth moments of the spectral distribution,[5] which indicate that the line shape is neither Lorentzian nor Gaussian. The real-time response function $F(t)$, the so-called free-induction-decay (FID) curve, derived from experiments[6] on CaF_2, was found by Abragam[7] to be accurately described by the function

$$F(t) = e^{-a^2t^2/2}\sin(bt)/bt\,, \tag{1.1}$$

when the parameters a and b were adjusted so to get the right second and fourth moments of the spectral function. In the early 1970s the calculation of the moments was extended to include the sixth and eighth,[8] and the method of Abragam was generalized in order to account for the values of these higher moments.[4,9] Experimentally, the FID curves of the standard NMR system CaF_2 were determined with very high precision by Engelsberg and Lowe.[10] Later on important progress in determining the response function from the equations of motion was made by Engelsberg and Chao,[11] by Becker *et al.*,[12] and by Lundin.[13,14] The method of Lundin, which has recently been developed further by Shakhmuratov,[15] is reminiscent of the simple physical interpretation made by Lefmann and collaborators of the double-peak structure in ^{13}C diamond, where the splitting is considered to be due to the strongly coupled pairs of nearest neighbors, and the width to a Gaussian-like distributed random field from other neighbors.[1,16]

In the present work the equations of motion of the Green function are analyzed. One main result is that, if only the z components of the spins are coupled, the Green function is to a very good approximation determined by a single-branched continued fraction, which may be computed accurately by numerical methods. This result is then generalized to include the effects of the x and y components of the dipole-dipole interaction. In this step, we utilize the analytic results obtained previously for the higher moments. A numerical analysis is then carried through in the cases corresponding to CaF_2 and ^{13}C diamond. The results obtained by the present method agree closely with the experimental results obtained for CaF_2. In the case of ^{13}C diamond there are discrepancies, which are probably mostly of experimental origin.

II. EQUATIONS OF MOTION

We want to consider the linear magnetic response of a lattice of nuclear moments subjected to a large stationary field. The normal situation in the case of a NMR experiment is that kT is much larger than the mean-field splitting between the nuclear levels, which is again much larger than the energy shifts due to the coupling between the nuclear moments. These conditions we shall assume to be satisfied throughout. We shall only treat the case

of $I = 1/2$ nuclei placed in a nonmetallic crystal. In this case we need only to consider the classical coupling of the nuclear moments and, neglecting nonlinear effects, the Hamiltonian may effectively be reduced to[7,17]

$$\mathcal{H} = -\frac{\Delta}{2}\sum_i \sigma_i^z - \sum_{ij} J_x(ij) s_i^+ s_j^- - \frac{1}{4}\sum_{ij} J_z(ij)\sigma_i^z\sigma_j^z \,. \tag{2.1}$$

$\Delta = g\mu_N H_z$ is the Zeeman splitting between the $I_z = \pm\frac{1}{2}$ states, g is the nuclear g factor, and the gyromagnetic ratio $\gamma = g\mu_N/\hbar$. The operators $s_i^{\pm} = I_{xi} \pm i I_{yi}$ and $\sigma_i^z = 2I_{zi}$. An effective dipole-coupling parameter is defined as

$$D_{ij} = \frac{3(1-3\cos^2\theta_{ij})}{4R_{ij}^3}(g\mu_N)^2 \,, \tag{2.2}$$

where R_{ij} is the distance between the ith and jth nucleus, and θ_{ij} is the angle between the line connecting the two nuclei and the z axis. The contribution of the dipole-dipole interaction is then included in Eq. (2.1) via

$$J_x(ij) = \tfrac{1}{3}D_{ij}, \quad J_z(ij) = -\tfrac{2}{3}D_{ij} \,. \tag{2.3}$$

The frequency-dependent Green functions are defined as

$$G(\hat{A}) = \lim_{\eta\to 0^+}\int_{-\infty}^{\infty}(-\tfrac{i}{\hbar})\theta(t)\Big\langle\Big[\hat{A}(t), \sum_j s_j^-\Big]\Big\rangle e^{i(\omega+i\eta)t}dt \,, \tag{2.4}$$

where $\theta(t)$ is the step function, and the equation of motion[18,19] is

$$\hbar\omega G(\hat{A}) - G([\hat{A},\mathcal{H}]) = \Big\langle\Big[\hat{A}, \sum_j s_j^-\Big]\Big\rangle \,. \tag{2.5}$$

Due to our general assumptions, we can neglect the dipole coupling in the determination of the thermal average on the RHS of this equation, and only $\langle[s_i^+, \sum_j s_j^-]\rangle = \langle\sigma_i^z\rangle \simeq \Delta/kT$ is nonzero to leading order in $1/kT$. The linear response observed in NMR experiments is proportional to the imaginary part of the Green function $G(s_i^+)$. Utilizing the special properties of the spin-1/2 operators, e.g., $(\sigma_i^z)^2 = 1$, Eqs. (2.1) and (2.5) lead to the following equation:

$$\varepsilon G(s_i^+) = -\langle\sigma_i^z\rangle + \sum_j [J_x(ij)G(\sigma_i^z s_j^+) - J_z(ij)G(s_i^+\sigma_j^z)] \tag{2.6}$$

with $\varepsilon = \Delta - \hbar\omega$. The next-order Green functions are determined by $(i \neq j)$

$$\begin{aligned}\varepsilon G(s_i^+\sigma_j^z) = {} & J_x(ij)G(s_j^+) - J_z(ij)G(s_i^+) + \sum_k{}' \Big[J_x(ik)G(\sigma_i^z\sigma_j^z s_k^+) - J_z(ik)G(s_i^+\sigma_j^z\sigma_k^z) \\ & + 2J_x(jk)\{G(s_i^+ s_j^+ s_k^-) - G(s_i^+ s_j^- s_k^+)\}\Big] \,,\end{aligned} \tag{2.7}$$

where the primed sum means that the summation index (k) has to be different from the other indices (i or j). Next we find, when all indices i, j, and k are different from each other,

$$\begin{aligned}\varepsilon G(s_i^+\sigma_j^z\sigma_k^z) = {} & J_x(ik)G(\sigma_j^z s_k^+) + J_x(ij)G(s_j^+\sigma_k^z) - J_z(ik)G(s_i^+\sigma_j^z) - J_z(ij)G(s_i^+\sigma_k^z) \\ & + \sum_l{}' \Big[J_x(il)G(\sigma_i^z\sigma_j^z\sigma_k^z s_l^+) - J_z(il)G(s_i^+\sigma_j^z\sigma_k^z\sigma_l^z) \\ & + 2J_x(jl)\{G(s_i^+ s_j^+\sigma_k^z s_l^-) - G(s_i^+ s_j^-\sigma_k^z s_l^+)\} + 2J_x(kl)\{G(s_i^+\sigma_j^z s_k^+ s_l^-) - G(s_i^+\sigma_j^z s_k^- s_l^+)\}\Big]\end{aligned} \tag{2.8}$$

and

$$\begin{aligned}2\varepsilon G(s_i^+ s_j^+ s_k^-) = {} & J_x(ik)\{G(\sigma_i^z s_j^+) - G(s_j^z\sigma_k^z)\} + J_x(jk)\{G(s_i^+\sigma_j^z) - G(s_i^+\sigma_k^z)\} \\ & + 2\sum_l{}' \Big[J_x(il)G(\sigma_i^z s_j^+ s_k^- s_l^+) + J_x(jl)G(s_i^+\sigma_j^z s_k^- s_l^+) - J_x(kl)G(s_i^+ s_j^+\sigma_k^z s_l^-) \\ & - \{J_z(il) + J_z(jl) - J_z(kl)\}G(s_i^+ s_j^+ s_k^-\sigma_l^z)\Big] \,.\end{aligned} \tag{2.9}$$

The major complications in the equations of motion above are due to $J_x(ij)$. The Green function $G_z(s_i^+)$, determined by these equations when $J_x(ij) \equiv 0$, only depends on higher-order Green functions $G_z(s_i^+\sigma_j^z\sigma_k^z\cdots)$ involving one s^+ operator, and in the next order:

$$\begin{aligned}\varepsilon G_z(s_i^+\sigma_j^z\sigma_k^z\sigma_l^z) = {} & -J_z(ik)G_z(s_i^+\sigma_j^z\sigma_l^z) \\ & - J_z(ij)G_z(s_i^+\sigma_k^z\sigma_l^z) \\ & - \sum_m{}' J_z(im)G_z(s_i^+\sigma_j^z\sigma_k^z\sigma_l^z\sigma_m^z) \,.\end{aligned} \tag{2.10}$$

Hence the hierarchy of Green functions determining $G_z(s_i^+)$ has a transparent structure, and Lowe and Norberg have found the exact solution for the real-time response function[20]

$$F(t) = \prod_j \cos\left(J_z(ij)t/\hbar\right) \tag{2.11}$$

from which $G_z(s_i^+)$ may be determined by a Fourier transformation. We shall not make use of this solution but rather consider the approximate one which is obtained if the first three terms of Eq. (2.10) are replaced by the single term $-3J_z(il)G_z(s_i^+\sigma_j^z\sigma_k^z)$. With a similar modification of all the equations of motion [the two terms in front of the summation sign of Eq. (2.8) are replaced by $-2J_z(ik)G_z(s_i^+\sigma_j^z)$] the equations are reduced to a set which only involves a single chain of Green functions. Introducing a vector with the components $G_z(s_i^+)$, $J_z(ij)G_z(s_i^+\sigma_j^z)$, $J_z(ij)J_z(ik)G_z(s_i^+\sigma_j^z\sigma_k^z)$, etc., these equations may be written as an infinite-dimensional matrix equation, for which an infinite continued fraction provides a solution

$$G_z(s_i^+) = \cfrac{-\langle\sigma_i^z\rangle}{\varepsilon - \sum_j \cfrac{J_z^2(ij)}{\varepsilon - \sum_k{}' \cfrac{2J_z^2(ik)}{\varepsilon - \sum_l{}' \cfrac{3J_z^2(il)}{\varepsilon - Q_4^z(ijkl)}}}} \tag{2.12}$$

with

$$Q_4^z(ijkl) = \sum_m{}' \frac{4J_z^2(im)}{\varepsilon - Q_5^z(ijklm)}, \tag{2.13}$$

etc. Notice that $Q_4^z(ijkl)$ depends implicitly on the indices j, k, and l, because the summation index m has to be different from all the preceding ones, as indicated by the prime. Equation (2.12) is the exact solution, if all nonzero values of $J_z(ij)$ are equal. In general it is not, but it is extremely close to it; the second, fourth, and sixth moments are correct, the eighth differs only minutely from its right value [at maximum 0.13% in the case of a cubic structure when $J_z(ij) \propto D_{ij}$], and the dominant contribution to all the $2n$th moments, proportional to the nth power of the second moment, is accounted for.

The response $G_z(s_i^+)$ is closely determined by the single-branched continued fraction above, and the conjecture is now that the final Green function, including the $J_x(ij)$ coupling, may to a good approximation still be written in this way, except that the dependence on the coupling parameters is altered, i.e., Q_p^z in (2.12) is replaced by

$$Q_p(ij\cdots) = \sum{}' \frac{X_p(ij\cdots)}{\varepsilon - Q_{p+1}(ij\cdots)}. \tag{2.14}$$

Dividing the numerator and denominator in Q_p with ε and performing a stepwise Taylor expansion, we find that the infinite continued fraction representing $G(s_i^+)$ may be written as a systematic expansion in odd powers of $1/\varepsilon$:

$$G(s_i^+) = -\frac{\langle\sigma_i^z\rangle}{\varepsilon}\left[1 + \frac{1}{\varepsilon^2}\sum_j{}' X_1(ij) + \frac{1}{\varepsilon^4}\sum_j{}' X_1(ij) \times\left\{\sum_{j'}{}' X_1(ij') + \sum_k{}' X_2(ijk)\right\} + \cdots\right]. \tag{2.15}$$

Assuming all nuclei to be placed in equivalent surroundings, i.e., $G(s_i^+) = G(s_j^+)$, then we get from Eqs. (2.6)–(2.9)

$$G(s_i^+) = -\frac{\langle\sigma_i^z\rangle}{\varepsilon}\left[1 + \frac{1}{\varepsilon^2}\sum_j D_{ij}^2 + \frac{1}{\varepsilon^4}\sum_j D_{ij}^2 \times\left\{\sum_{j'} D_{ij'}^2 + \frac{1}{9}\sum_k{}'(7D_{ik}^2 + 5D_{jk}^2 + 6D_{ik}D_{kj})\right\} + \cdots\right] \tag{2.16}$$

utilizing that the summation indices may be interchanged (the prime on the j sums is unnecessary as $D_{ii} = 0$). A comparison of (2.15) and (2.16) then allows the identification of X_1 and X_2. The distinction between D_{ik}^2 and D_{jk}^2 in the last sum is arbitrary, and because $G(s_i^+) = (1/N)\sum_i G(s_i^+)$ the result should be the same if the sum over j, in the first step of the infinite continued fraction, is replaced by a sum over i. In order to ensure this, also when introducing the higher-order terms, it is sufficient to assume the solution to be symmetric in i and j:

$$X_1(ij) = D_{ij}^2, \tag{2.17a}$$

$$X_2(ijk) = \frac{2}{3}\left\{D_{ik}^2 + D_{jk}^2 + D_{ik}D_{kj}\right\}. \tag{2.17b}$$

The moments of the spectral energy distribution, defined with respect to the mean value Δ, are

$$M_n = \langle\varepsilon^n\rangle = \int_{-\infty}^{\infty} \varepsilon^n G''(s_i^+;\varepsilon)d\varepsilon \Big/ \int_{-\infty}^{\infty} G''(s_i^+;\varepsilon)d\varepsilon, \tag{2.18}$$

where $G''(s_i^+;\varepsilon)$ denotes the imaginary part of the Green function [M_n is $(2\pi\hbar)^n$ times the usual frequency moments]. The odd moments vanish by symmetry, and an elementary result is

$$G(s_i^+) = -\frac{\langle\sigma_i^z\rangle}{\varepsilon}\left[1 + \frac{1}{\varepsilon^2}M_2 + \frac{1}{\varepsilon^4}M_4 + \cdots\right], \tag{2.19}$$

which shows that (2.16) is equivalent to an expansion of $G(s_i^+)$ in terms of the spectral moments. Introducing the notation $S_n = \sum_j D_{ij}^n$, the moments are

$$M_2 = S_2, \tag{2.20a}$$

$$M_4 = \frac{1}{3}\left\{7S_2^2 - 4S_4 + 2S_2\sum_k D_{ik}D_{kj}\right\}, \tag{2.20b}$$

in accordance with previous results.[5,8]

The complexity in performing the expansion (2.16) of $G(s_i^+)$ increases dramatically in the next order. Therefore we make use of the additional assumption that terms which involve products of two different D couplings can be neglected in X_p, when $p \geq 3$. The coupling D_{ij} takes on both positive and negative values and D_{ij} integrated over a sphere vanishes, whereas in contrast D_{ij}^2 is always positive. Advancing one more step in the hierarchy of Green functions, beyond that of Eqs. (2.8) and (2.9), and keeping track of only the squared coupling terms, we find the linear combination $X_3(ijkl) = aD_{il}^2 + bD_{jl}^2 + cD_{kl}^2$ to be determined by $a + b + c = 41/18$, and further that a solution symmetric in i and j ($a = b$) implies $c = 0$, thus

$$X_3(ijkl) = \frac{41}{36}\{D_{il}^2 + D_{jl}^2\}. \tag{2.21}$$

This result predicts the sixth moment M_6 to be

$$\frac{1}{27}\left\{229S_2^3 - 373S_2S_4 + 171S_6 - 41\sum_{jk} D_{ij}^2 D_{ik}^2 D_{kj}^2\right\}$$

plus the terms deriving from $D_{ik}D_{kj}$ in $X_2(ijk)$, which is consistent with the analytical result for M_6 derived by Knak Jensen and Kjærsgård Hansen.[8] It is possible to include most of the terms in M_6 depending on the linear factors, but the price is that $Q_2(ij)$ has to be divided into at least two continued fractions, which makes the procedure somewhat arbitrary. More importantly, in principle, is the occurrence[8] of the term $-(8/27)\sum D_{ij}D_{ik}D_{il}D_{lk}D_{kj}D_{jl}$ in M_6. It falls outside the present scheme and cannot be incorporated into the continued fraction in any simple way, thus indicating a limit to the present procedure. However, as discussed above, the contributions to M_6 which are neglected in Eq. (2.21) are expected to be small, and this is supported by the numerical analysis discussed below.

In the higher order it is not important to discriminate between the different quadratic contributions, e.g., between D_{im}^2, D_{jm}^2, ... in $X_4(ijklm)$. In any case, such a separation plays no role in the following numerical analysis, and we may assume

$$X_p(ijk\cdots\gamma) = \frac{\alpha_p}{2}\{D_{i\gamma}^2 + D_{j\gamma}^2\}, \quad p \geq 4 \tag{2.22}$$

corresponding to Eq. (2.21). Using the result of Knak Jensen and Kjærsgård Hansen[8] that the leading order term in M_8 is $(11\,031/243)S_2^4$, we find $\alpha_4 = 2819/738$. Introducing an effective α_p for the lower-order terms also, we get the following sequence of values for α_p:

$$1, \quad \frac{4}{3}, \quad \frac{41}{18}, \quad \frac{2819}{738}$$

for $p = 1$, 2, 3, and 4. The final Green function is not much dependent on how the series is continued, except that α_p increases with p [which is guaranteed by the $J_z(ij)$ coupling]. Although the four moments M_2–M_8 do not determine the response, they put strong limits on the kind of variation which may be achieved by varying the higher-order terms. However, our ignorance of how the α_p series continues leaves us a single degree of freedom, which we have utilized for a small overall adjustment of the calculated response functions, using for this purpose the accurate experimental results for CaF_2. We have tried to use linear extrapolations [$\alpha_p = 1 + 1.16(p-1)$ or $\alpha_p = \alpha_4 + 2.2(p-4)$], but the α_p values above are described closely by $\alpha_p = 1 + 0.033(p-1) + 0.302(p-1)^2$, i.e., α_p seems to increase quadratically rather than linearly with p, and we obtained a slightly better result by using the following quadratic extrapolation:

$$\alpha_p = 1 + 0.327(p-1)^2, \quad p \geq 5. \tag{2.23}$$

In the numerical evaluation of the Green function we have to make some additional approximations. The infinite continued fraction

$$G(s_i^z) = \cfrac{-\langle\sigma_i^z\rangle}{\varepsilon - \sum_j \cfrac{D_{ij}^2}{\varepsilon - Q_2(ij)}} \tag{2.24}$$

becomes less and less dependent on the actual values of $Q_p(ij\cdots)$ the larger p is, and to a first approximation we assume that the summation index only needs to be different from i and j. In this approximation $\sum{}' X_p(ijk\cdots\gamma) \simeq \alpha_p V(ij)$ with $V(ij) = S_2 - D_{ij}^2$ for $p \geq 3$, hence

$$Q_2(ij) \simeq \cfrac{\frac{4}{3}V(ij) + \frac{2}{3}\sum_k D_{ik}D_{kj}}{\varepsilon - \cfrac{\alpha_3 V(ij)}{\varepsilon - \cfrac{\alpha_4 V(ij)}{\varepsilon - \ddots}}}. \tag{2.25}$$

The infinite continued fraction has to be determined for each value of the summation index j. This is done by assuming α_p to be constant for $p \geq n$, i.e., $Q_n(ij) \simeq \alpha_n V(ij)/\{\varepsilon - Q_n(ij)\}$ or

$$Q_n(ij) = \frac{1}{2}\left\{\varepsilon - \sqrt{\varepsilon^2 - 4\alpha_n V(ij)}\right\}. \tag{2.26}$$

The minus sign in front of the square root is the only choice which leads to the right sign of $G''(s_i^+)$. Even for rather large values of n, this termination of the infinite continued fraction gives rise to spurious oscillations in the calculated response function (as function of n or ε), which are, however, found to cancel out in the mean value of the response function calculated for two successive values of n. With the use of this averaging procedure it is found that the result becomes independent of n, when n is larger than about 20–30 (we have used $n = 50$ and 51 in the final calculations). The approximation made in Eq. (2.25) for $Q_2(ij)$ may be improved, and to next order we get

$$Q_2(ij) = \frac{2}{3}\sum_k{}' \cfrac{D_{ik}^2 + D_{jk}^2 + D_{ik}D_{kj}}{\varepsilon - \cfrac{\alpha_3 W(ijk)}{\varepsilon - \cfrac{\alpha_4 W(ijk)}{\varepsilon - \ddots}}} \tag{2.27}$$

with $W(ijk) = S_2 - D_{ij}^2 - (D_{ik}^2 + D_{jk}^2)/2$. The effective coupling parameter D_{ij}^2 is proportional to R_{ij}^{-6}, but although this coupling decreases much faster than the dipole coupling itself, the j sum has to be extended over 10–20 000 neighbors in order to obtain an acceptable accuracy. Fortunately, the modifications introduced by the replacement of Eq. (2.25) by Eq. (2.27) only influence the final response function weakly, and it is only necessary to apply the improved expression for $Q_2(ij)$ when j is one of the 20–30 neighbors which are coupled most strongly to the ith site. The result (2.27) may be considered to correspond to the analytical result derived above. The next step, which involves taking into account that the summation indices in $Q_4(ijkl)$ have to be different from l, presupposes a more detailed determination of $X_4(ijklm)$ than given by Eq. (2.22), and requires much more extensive numerical calculations. Considering Eq. (2.27) to be the starting equation, we may say in short that all additional approximations made in the numerical analysis are kept at such a level that their influence on the final results is insignificant.

III. COMPARISON WITH EXPERIMENTS

A. Calcium fluoride

CaF_2 has for a long time served as a standard material for comparisons between NMR line-shape theories and experiments.[7,10] The stable ^{19}F isotope in CaF_2 with $I = 1/2$ and $g = 5.254\,54$ ($\gamma = 25\,166.2$ rad s^{-1} Oe^{-1}) is positioned on a simple cubic lattice with the lattice parameter $a/2 = 2.723\,25$ Å in the low-temperature limit.[10] The nuclear magnetic resonance in CaF_2 was measured by Bruce in 1957 with the field applied along the three high symmetry directions,[6] and 14 years later Engelsberg and Lowe repeated the measurements and established with a high degree of accuracy the FID curve in each of the three cases.[10] We have used their parametrized experimental results for calculating the corresponding Fourier-transformed response functions which are shown in Fig. 1. These results should benefit from the great precision by which the FID curves were measured, and it has been checked that the moments of the resonance curves (up to the eighth) are those reported[10] by Engelsberg and Lowe in their Table IV. The results of Bruce,[6] in the cases where the field is along [100] or [110], agree well with those derived from the experimental FID curves of Engelsberg and Lowe, when the data are corrected for the change of the lattice constant which occurs between room temperature and 4.2 K. Bruce's result in the case of a field along [111] has a second moment which is about 13% larger than the theoretical value,[21] but a folding of the results of Engelsberg and Lowe with a Gaussian with a width which corrects for the difference between the second moments leads to a good coincidence of the two sets of experimental results in this case also.

The experimental results in Fig. 1 are compared with the predictions of Eq. (2.27). The intensities shown in the figure are $-(g\mu_N/\langle\sigma_i^z\rangle)G''(s_i^+)$ as functions of the field parameter $\varepsilon/g\mu_N$, and the experimental results have been scaled so that the total integrated intensity is equal to π in all the cases shown. As may be seen in the figure, the agreement between theory and experiment is very good, but there are small systematic deviations, which are at most 2–3 % of the intensity at zero frequency. Figure 2 shows a blowup of the intensity differences between the experimental results and the theory in CaF_2. It is difficult to determine the origin of these deviations, but they are most likely due to the approximations made in the theory rather than to the experimental uncertainties.

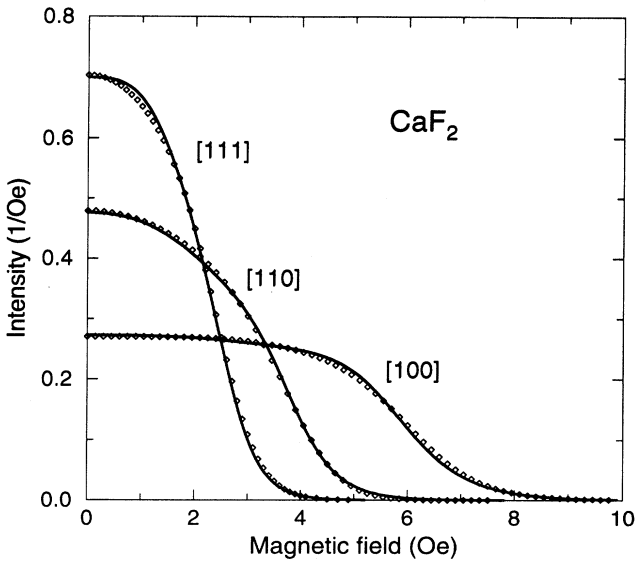

FIG. 1. The NMR line shape in CaF_2 when the field is along one of the three high symmetry directions, shown as a function of the field parameter $\varepsilon/g\mu_N$. The symbols indicate the experimental results derived from the parametrized FID curves of Engelsberg and Lowe (Ref. 10) and the solid lines are the theoretical predictions.

The corresponding spectral moments are given in Table I. The experimental moments M_2 ($\widetilde{M}_2 = M_2/g\mu_N$ in

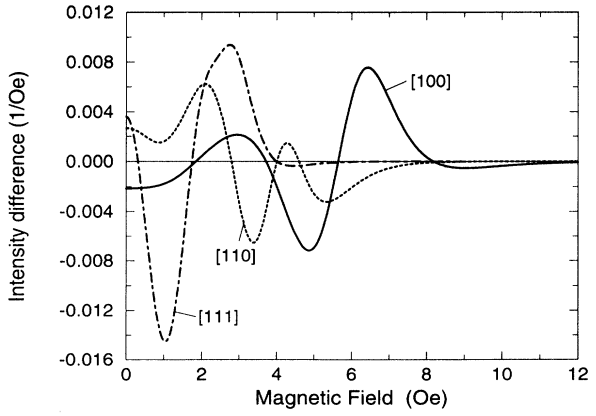

FIG. 2. The intensity difference in CaF_2 between the experimental and theoretical results in Fig. 1.

TABLE I. The spectral moments in CaF_2. The experimental values are derived from the parametrized FID curves of Engelsberg and Lowe (Ref. 10), and the exact values of M_6 and M_8 are the results of Knak Jensen and Kjærsgård Hansen (Ref. 8), extrapolated to the infinite lattice. M_2 is the same in each row of the table.

		$\widetilde{M}_2^{1/2}$ (Oe)	M_4/M_2^2	M_6/M_2^3	M_8/M_2^4
[100]	Expt.	3.615	2.103	6.08	22.2
	Theory	3.6020	2.1244	6.427	26.57
	Exact	3.6021	2.1245	6.329	25.16
[110]	Expt.	2.191	2.236	6.93	26.7
	Theory	2.2174	2.3021	7.815	36.85
	Exact	2.2176	2.3022	7.709	34.96
[111]	Expt.	1.508	2.340	8.05	36.9
	Theory	1.4937	2.3693	8.540	43.78
	Exact	1.4940	2.3694	8.511	44.09

Table I) and M_4 are in good agreement with the theoretical values. M_6/M_2^3 and M_8/M_2^4, which are determined with experimental uncertainties of, respectively, about 7% and 15%, are systematically smaller than predicted by the theory. However, one should take into consideration that the exponentially decaying tail, in for instance the [111] case above a field of 9.5 Oe, accounts for 0.1% of the intensity but contributes as much as 11% and 26% to, respectively, the sixth and the eighth moments. Actually, we may say that the parametrized experimental results of Engelsberg and Lowe, including an extrapolation of the long-time behavior of the FID curves, account for a surprisingly large portion of the tails. Concerning the comparison between the moments predicted by the present theory and the in principle exact values obtained by a direct calculation of the moments, we remark first that, since the theory should predict the right second and fourth moments, the close coincidence seen for these moments just reflects the accuracy of the numerical analysis. Second, we notice that the values of M_6 and M_8 predicted by the theory only differ from the exact values by a few percent, which shows that the terms discarded in the expression for $X_3(ijk)$ or $X_4(ijkl)$, (2.21) or (2.22), only have minor effects on these moments.

The free-induction-decay curve is defined as the (normalized) time-dependent correlation function of the averaged I_x component in the rotating frame set up by the stationary field, which may be shown to be[7]

$$F(t) = \int_{-\infty}^{\infty} G''(s_i^+;\varepsilon)\cos(\varepsilon t/\hbar)d\varepsilon \Big/ \int_{-\infty}^{\infty} G''(s_i^+;\varepsilon)d\varepsilon\,. \tag{3.1}$$

The FID curve in the case of a field along [100] predicted by the theory is compared with the experimental (parametrized) FID curve observed by Engelsberg and Lowe[10] in Fig. 3. The agreement is close for times less than 50 μs. At longer times some discrepancies develop and the times at which the FID curve becomes zero are about 5–6 % larger than observed experimentally. The period of the oscillations is greater when the field is applied along the other symmetry directions, and here the calculated positions of the zeros agree within 3–4 % with the experimental values. The long-time form of the FID curve is well described by the simpler exponentially decaying function[10]

$$F(t) \approx Ae^{-\alpha t}\cos(\beta t + c)\,,$$

instead of expression (1.1) introduced by Abragam, and the theoretical values of parameters α and β are compared with experiment in Table II.

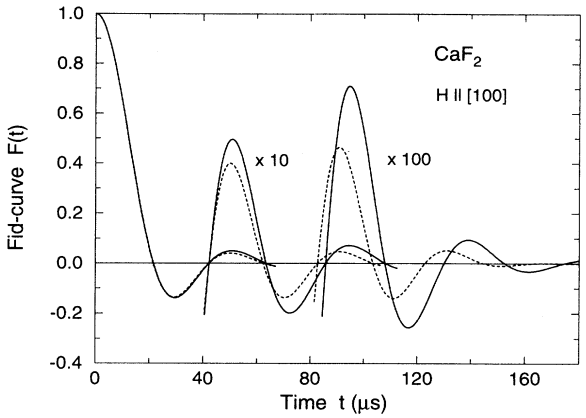

FIG. 3. The FID curve $F(t)$ in CaF_2 when the field is along [100]. The dashed lines are the experimental results of Engelsberg and Lowe (Ref. 10) and the solid lines are the theoretical results.

B. ^{13}C diamond

The present work was initiated by the NMR experiments of Lefmann *et al.*[1] on ^{13}C diamond. However, the experimental conditions were less favorable in this system and the results therefore not of the same high accuracy as in CaF_2. The $I = 1/2$ carbon nucleus ^{13}C has $g = 1.404\,37$ ($\gamma = 6726.1$ rad s^{-1} Oe^{-1}) and is placed in a diamond lattice with the lattice parameter $a = 3.5666$ Å at room temperature. The diamond lattice is not a Bravais lattice, but the inversion symmetry between the two fcc sublattices implies that the surroundings of each nuclei are equivalent, and the theory is directly applicable also in this case. The theoretical resonance curves $-(2\pi\hbar/\langle\sigma_i^z\rangle)G''(s_i^+)$ as functions

TABLE II. Parameters of the long-time form of the FID curves in CaF_2. The experimental values are from Ref. 10.

	α (calc.) (μs^{-1})	α (expt.) (μs^{-1})	π/β (calc.) (μs)	π/β (expt.) (μs)
[100]	0.064	0.050	22.2	20.5
[110]	0.043	0.041	32.8	30.6
[111]	0.029	0.030	46.1	47.6

of frequency $\varepsilon/2\pi\hbar$, when the field is applied along the three symmetry directions, are compared with the experimental results in Fig. 4. It is immediately seen that, although the qualitative behavior is similar, the experimental widths of the resonance curves are considerably larger than the theoretical ones. This is also clearly reflected in the spectral moments given in Table III (here $\widetilde{M}_2 = M_2/2\pi\hbar$). The experimental second moments were calculated by Lefmann *et al.*, and we also give the values of the experimental fourth moments estimated from the resonance curves in Fig. 4. In addition to the theoretical second and fourth moments, which are equal to the exact values, we also give the calculated values of the sixth and eighth moments, which are expected to be correct within a few percent.

A comparison of the tabulated moments shows that the ratio between the second and the higher moments in CaF_2, when the field is along [111] and [110], are nearly the same as in ^{13}C diamond when the field is along, respectively, [100] and [110]. This coincidence is also found to occur for the calculated line-shape curves (most pronouncedly in the first of the two cases), if the square roots of the second moments are used as scale parameters.

The experiment shows that the resonance line in the [111] case splits into two peaks, as also predicted by the theory. The calculated splitting of the resonance line is 8.56 kHz, which is near to the observed value. Based on Eqs. (2.24)–(2.25), it is found that the parameter which is decisive for the occurrence of the splitting is the minimum

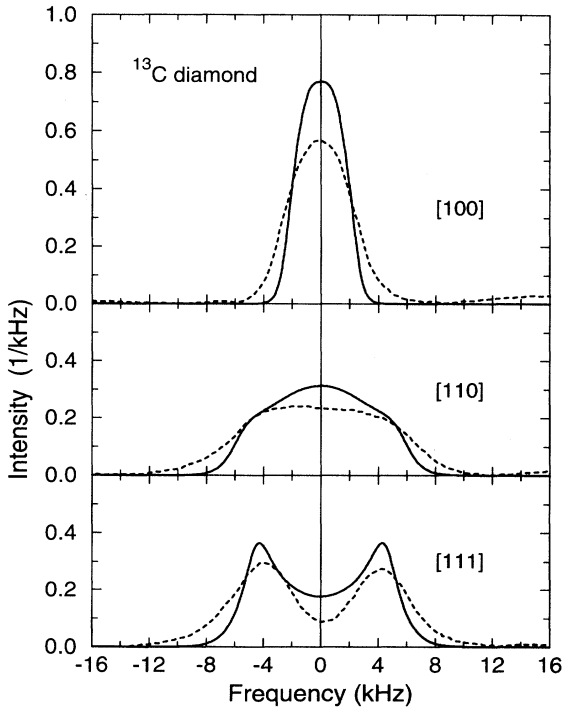

FIG. 4. The NMR resonance line in ^{13}C diamond as a function of $\varepsilon/2\pi\hbar$ when the field is along [100], [110], and [111]. The dashed lines show the experimental results of Lefmann *et al.* (Ref. 1) and the solid lines are the theoretical curves.

TABLE III. The spectral moments in ^{13}C diamond. The experimental values are from Ref. 1.

		$\widetilde{M}_2^{1/2}$ (kHz)	M_4/M_2^2	M_6/M_2^3	M_8/M_2^4
[100]	Expt.	2.1	3.7		
	Theory	1.3710	2.3906	8.728	45.46
[110]	Expt.	4.5	2.5		
	Theory	3.4294	2.2419	7.139	30.43
[111]	Expt.	5.0	2.0		
	Theory	3.8800	1.7822	4.471	15.89

value of the ratio

$$r(ij) = \tfrac{4}{3}\left\{S_2 - D_{ij}^2 + \frac{1}{2}\sum_k D_{ik}D_{kj}\right\}/S_2 . \qquad (3.2)$$

In ^{13}C diamond in the [111] case the minimum value is found to be 0.43 for the two nearest neighbors along the direction of the field. The resonance in CaF_2 when the field is along [100] is just on the threshold where it splits into two peaks, and here the minimum value is 0.94, slightly smaller than 1, valid for the four nearest neighbors in the plane perpendicular to the field. In any of the other cases considered in the two systems the minimum ratio is larger than 1. Neglecting the last term in the numerator, the condition is approximately $4D_{ij}^2 > S_2$, i.e., the square of the coupling between one pair of the nuclear dipoles should contribute more than one-quarter of the total sum of the squared couplings, to be able to establish a coherent response of the dipole pair which is sufficiently strong to survive the incoherent effects due to other neighbors.

The comparison between theory and experiment in ^{13}C diamond shows that the experimental NMR line shapes are distorted. The only additional effects which may influence the results are the presence of impurities, or the repetition rate of 3–4 spectra per minute used in the experiment, which is relatively high compared with the long spin-lattice relaxation time of 14–16 s. To a first approximation the impurities give rise to an extra Gaussian broadening of the spectra. This is concordant with the results obtained in the [100] case, which correspond to the theoretical curve folded with a Gaussian with $\sigma = 1.6$ kHz, but the differences in the two other cases are not describable in this manner, which indicates that the high repetition rate might have had some influence on the results.

IV. DISCUSSION AND CONCLUSION

The NMR line shape due to the dipole coupling of $I = 1/2$ nuclei has been calculated approximately at high temperatures and high fields. The result is determined in terms of an infinite continued-fraction, which is relatively easy to handle by numerical methods. The spectra derived by the present theory have the right second and fourth moments, and the sixth and eighth moments

are found to be close to the values[8] calculated directly in the case of a simple cubic system. The theoretical results agree satisfactorily with the precise experimental results[10] of Engelsberg and Lowe for the FID curves in CaF_2 obtained with the field along each of the three high symmetry directions. In the case of ^{13}C diamond the theory predicts a splitting of the resonance line in the [111] case which is of the same size as observed by Lefmann *et al.*,[1] but the spectra are in general predicted to be more distinct than observed experimentally. The differences are believed to be mostly due to experimental difficulties, and the high repetition rate applied in the experiment, relatively to the spin-lattice relaxation time, is suggested to be a main cause.

The present theory may be considered to be a further development of the theory of Engelsberg and Chao[11] who derived an infinite continued-fraction representation for the Green function with $\sum' X_p(ij\cdots)$ in Eq. (2.14) replaced by constants deriving from the moments so that the expansion (2.19) is fulfilled, i.e., by the parameter $1/\tau_{p-1}\tau_p$ (τ_p is defined in their paper), where $1/\tau_0\tau_1 = M_2$, $1/\tau_1\tau_2 = (M_4 - M_2^2)/M_2$, etc. The termination of the infinite continued fraction was performed in the same way as here, Eq. (2.26), but only the known part of the fraction was included, i.e., they assumed $\tau_{p-1}\tau_p = \tau_3\tau_4$ for $p \geq 4$. The results derived by the two methods are nearly identical if the termination is introduced after step $n = 4$ in both cases (if the moments are the same). As discussed in connection with Eq. (2.26) the termination of the continued fraction at small values of n leads to spurious oscillations in the calculated response function. In the case of CaF_2 with the field applied along [100] the use of the exact moments produces oscillations of a magnitude which is about five times larger than those shown in Fig. 2. The magnitude of these oscillations may be controlled by τ_4 and with a slight reduction of M_8/M_2^4 from 25.2 to 23.2 (plus a minor adjustment of M_6) Engelsberg and Chao did reduce the magnitude of the oscillations by a factor 2–3. The previous theory thus relies on (small) adjustments of the sixth and eighth moments in order to reduce the spurious oscillations, which introduces some uncertainties in its predictions. Here we find that the proper way to control the oscillations is to extend the continued fraction further before it is terminated. The way this is done is not of particular importance, except that α_p in Eq. (2.22) has to increase with p. For instance, considering the linear extrapolation $\alpha_p = \alpha_4 + c(p-4)$, then the oscillations are reduced to the level obtained by Engelsberg and Chao, if c is about 1.5 or about 3, and in the middle of this interval the magnitude of the oscillations is reduced further by a factor 2–3. In this case, $c = 2.2$, the calculated spectra are all practically identical with those obtained on the basis of the quadratic extrapolation (2.23).

The present method bears some resemblance with the procedure of Parker and Lado,[4,9] who utilized the moment expansion directly for a calculation of the line-shape curves. The results obtained by the two methods are also quite similar but, considering the behavior of the FID curves at long times, Table II, the lengths of the periods predicted by the present theory are closer to the experimental values than those obtained by Parker and Lado. The zeros of the [100] FID curve in CaF_2 predicted by the approximate solution derived by Becker *et al.* of the equations of motion agree even more closely with experiment.[12] On the other hand their values for the moments, beyond the second, are systematically smaller than the correct values, which is probably mostly due to their neglect of terms involving more than one s^+ operator like the Green function $G(s_i^+ s_j^+ s_k^-)$ in Eq. (2.9). The method of Lundin[13,14] is based on a small number of assumptions which appear to be nearly fulfilled, and the improvements introduced by Shakhmuratov[15] lead to an excellent description of the [100] FID curve in CaF_2.

The infinite-continued-fraction solution derived in the present work may be improved in various ways. The most obvious one would be to include some of those terms neglected in X_3 and X_4. We have made some effort in this direction, but the improvements obtained were small and not commensurate with the extra complications appearing in the expression for the Green function and in the numerical work. In any case they are more or less eliminated by the arbitrariness connected to the extrapolation (2.23) of α_p beyond $p = 4$, which indicates that a further improvement in the theory would have to include a determination of α_5, in order to reduce the importance of the assumption about the behavior of the α_p series.

ACKNOWLEDGMENTS

The author would like to thank K. Lefmann and collaborators for providing him with the results of their measurements on ^{13}C diamond before publication. Useful discussions with K. Lefmann, F. Berg Rasmussen, and A. R. Mackintosh are gratefully acknowledged.

[1] K. Lefmann, B. Buras, E. J. Pedersen, E. S. Shabanova, P. A. Thorsen, F. B. Rasmussen, and J. P. F. Sellschop, Phys. Rev. B **50**, 15 623 (1994).
[2] G. E. Pake, J. Chem. Phys. **16**, 327 (1948).
[3] B. Pedersen and D. F. Holcomb, J. Chem. Phys. **38**, 61 (1963).
[4] G. W. Parker and F. Lado, Phys. Rev. B **8**, 3081 (1973).
[5] J. H. Van Vleck, Phys. Rev. **74**, 1168 (1948).
[6] C. R. Bruce, Phys. Rev. **107**, 43 (1957).
[7] A. Abragam, *The Principles of Nuclear Magnetism* (Oxford University Press, London, 1961), Chap. 4.
[8] S. J. Knak Jensen and E. Kjærsgård Hansen, Phys. Rev. B **7**, 2910 (1973).
[9] G. W. Parker and F. Lado, Phys. Rev. B **9**, 22 (1974).

[10] M. Engelsberg and I. J. Lowe, Phys. Rev. B **10**, 822 (1974).
[11] M. Engelsberg and N.-C. Chao, Phys. Rev. B **12**, 5043 (1975); N.-C. Chao and M. Engelsberg, *ibid.* **14**, 271 (1976).
[12] K.W. Becker, T. Plefka, and G. Sauermann, J. Phys. C **9**, 4041 (1976).
[13] A. A. Lundin and A. V. Makarenko, Zh. Eksp. Teor. Fiz. **87**, 999 (1984) [Sov. Phys. JETP **60**, 570 (1984)].
[14] A. A. Lundin, Zh. Eksp. Teor. Fiz. **102**, 352 (1992) [Sov. Phys. JETP **75**, 187 (1992)].
[15] R. N. Shakhmuratov, J. Phys. Condens. Matter **3**, 8683 (1991).
[16] K. Schaumburg, E. S. Shabanova, and J. P. F. Sellschop, J. Magn. Res. A **112**, 176 (1995).
[17] C. P. Slichter, *Principles of Magnetic Resonance*, 3rd ed. (Springer-Verlag, New York, 1990).
[18] D. N. Zubarev, Usp. Fiz. Nauk **71**, 71 (1960) [Sov. Phys. Usp. **3**, 320 (1960)].
[19] J. Jensen and A. R. Mackintosh, *Rare Earth Magnetism: Structures and Excitations* (Oxford University Press, Oxford, 1991), Chap. 3.
[20] I. J. Lowe and R. E. Norberg, Phys. Rev. **107**, 46 (1957).
[21] The theoretical values given by Bruce (Ref. 6) are obtained using a lattice parameter of $a/2 = 2.72$ Å (about 0.4% too small) and Eq. (13) in the paper of Van Vleck (Ref. 5), which can be replaced by the following more accurate version: $\langle \Delta\nu^2 \rangle_{\rm av} = 37.326 g^4 \beta^4 h^{-2} d^{-6} [\frac{1}{3} S(S+1)][(\lambda_1^4 + \lambda_2^4 + \lambda_3^4) - 0.194\,83]$.